The 2010 IEEE/RSJ International Conference on
Intelligent Robots and Systems
October 18-22, 2010, Taipei, Taiwan

Identification and experimentation of an industrial robot operating in varying-impedance environments

Xavier Lamy, Frédéric Colledani, Per-Olof Gutman, Senior *Member, IEEE*

Abstract— **It is well-known that iff the robot with its end-effector force control is passive, the closed loop system consisting of the robot and an arbitrary passive environment is asymptotically stable. Passive robot control, however, limits the achievable robot impedance reduction. Recently, [1] investigated what performance can be achieved with non-passive control when uncertainty bounds for the environment are known. The question of stability margins neglected in [1] is treated in our companion paper [2].**

In this paper we report on experiments on a full scale industrial robot in order to identify six transfer functions from the velocity reference of the inner velocity loop to the end effector force output for six different environments, from solid wall to air. It is shown how the experimental data also makes it possible to compute the impedance of the controlled robot. Two controllers are designed: one marginally stable but with non-passive and low-gain controlled robot impedance at low frequencies, and another controller respecting the stability margin of closed loop sensitivity gain less than 6 dB, but with a passive controlled robot impedance that has higher gain for low frequencies than that of the first controller.

The designs are compared experimentally by having the robot interact with environments of different impedances, and with a human operator leading the robot.

The paper is concluded by a short discussion of the possible need of controller adaption when a robot operates in varying impedance environments, and interacts with a human operator.

I. Introduction

THE interaction between a robot and its environment continues to be the subject of active research [3], [4], [5], including the interaction between a robot and a human operator, called *cobotics* or co-manipulation [6], [7], [1] [8]. A conceptual example is given in Figure 1, where a butcher directs a robot which augments to the meat cutting knife the force applied by the butcher to the robot handle. Such a configuration could be seen as a cascaded master-slave control system, where the outer loop is closed by the human operator who gives a force reference to the inner loop that includes the robot controller, the robot, and the work piece (piece of meat in Figure 1). Clearly, the robot controller "sees" an uncertain control object, since the dynamics of the environment (human operator and the work piece) might vary or change. Also when the robot functions autonomously without the interaction of the human operator, the control object is uncertain. It is thus mandatory to design the robot controller such that the closed loop system remains stable for the full range of given environment dynamics.

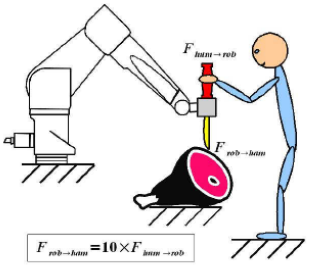

Fig. 1. Conceptual configuration of an industrial robot used as a human force augmentation system.

In the robotics literature the environment is characterized by its impedance [9]. Often it is passive, e.g. in the case of a piece of meat. Also the human operator impedance is considered passive [10]. It is well-known that if and only if the robot with its end-effector force control is passive, the closed loop system consisting of the robot and an arbitrary passive environment is asymptotically stable [11]. Passive robot control, however, limits the achievable robot impedance reduction which is an important performance criterion for co-manipulation [12]. Recently, [1] investigated what performance can be achieved with non-passive linear control when uncertainty bounds for the environment are known, but unfortunately neglected stability margins, and presented a marginally stable closed loop system. In the companion paper [2] we present a linear robust force control design with acceptable stability margins for the example in [1].

Manuscript received 28 February, 2010. This work was supported by the French Atomic Energy Commission (CEA).

Xavier Lamy is a PhD student with the French Atomic Energy Commission (CEA), Software Intensive Systems Department (LIST), Interactive Robotics Laboratory, 92265 Fontenay-aux-Roses, France, and with University of Paris 6 - UPMC, Insitut des Systèmes Intelligents et de Robotique (CNRS - FRE 2507) (email: xavier.lamy@cea.fr).

Frédéric Colledani is with CEA, LIST, Interactive Robotics Laboratory, 92265 Fontenay-aux-Roses, France (e-mail: frederic.colledani@cea.fr).

Per-Olof Gutman is with CEA-LIST DTSI/ Interactive Robotics Laboratory, 92265 Fontenay-aux-Roses, France, on sabbatical leave 2009-2010 from the Faculty of Civil and Environmental Engineering, Technion – Israel Institute of Technology, Haifa 32000, Israel (tel: +33 6 88509325, e-mail: peo@cea.fr, peo@technion.ac.il).

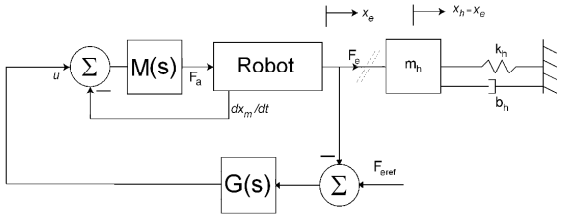

Fig. 2. Block diagram of the closed loop robot system with uncertain environment, the latter modeled, to the right of //, as a passive system with a spring k_h [Nm/rad], moment-of-inertia m_h [kg·m^2], and damper b_h [Nm/(rad/s)] whose parameters are uncertain or vary. x_h [rad] is the position of the environment that equals the robot end effector position x_e [rad]. F_e [Nm] is the torque exerted by the robot on the environment, and is the measured plant output controlled by the main controller whose transfer function is G(s). F_{eref} [Nm] is the torque reference of the main control loop, and is often set to 0. The robot has a built-in inner motor velocity control loop, where dx_m/dt [rad/s] is the motor angular velocity, and F_a [Nm] is the torque commanded by the motor velocity controller M(s). The motor velocity reference u [rad/s] is generated by the torque controller G(s). With G(s)=0, the system operates with the motor velocity loop, only.

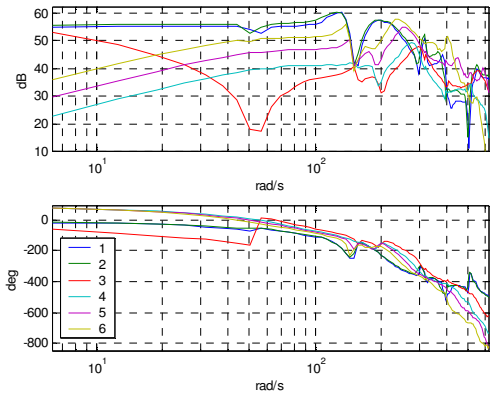

Fig. 3. Six experimentally measured frequency response functions, $P_i(j\omega)$, i=1,…,6 for the Stäubli RX90L robot attached to environments described in section V. $P_1(j\omega)$ is chosen as the nominal.

Robust force control was investigated experimentally using a Stäubli RX90L robot operating in a one degree-of-freedom rotational mode, with its end-effector interacting with different environments. The robot is equipped with an inner motor velocity loop, so that the control signal is the motor velocity reference. Six different plant transfer functions from velocity reference to the measured end-effector torque output were identified by frequency response measurements. Based on the method in [13] and further expounded here, the impedance of the robot with force feedback control was computed.

Two controllers were designed and investigated experimentally. According to the measurement based calculations, the conventional PI-controller $G_X(s)$ makes the controlled robot impedance marginally non-passive, and the closed loop marginally stable. The sixth order linear controller $G_P(s)$ respects the stability margin $|S_i(s)|\leq 6$ dB, i=1,…6, where S stands for the closed loop sensitivity function, and i is the environment index, and makes the controlled robot impedance passive.

It is not surprising that $G_X(s)$ gives desirable controlled robot impedance with lower gain at low frequencies. The conclusions section discusses how to mitigate the price, being marginal closed loop stability apparent in some environments, by controller adaptation.

II. Identification Experiments

The two-link arm of a Stäubli RX90L robot were aligned along one line in a horizontal plane, perpendicular to the main vertical axis of the robot, around which the robot was allowed to rotate. The robot is equipped with an inner motor velocity loop, so its velocity reference equals the control signal u(t), see Figure 2. With G(s)=0, six different plant transfer functions from the velocity reference u(t) to the measured end-effector torque output $F_e(t)$ were identified by frequency response measurements and the Fourier integral method [14], sampled at 341.3 Hz, for 1, 2, 3, …, 97, 98, 99 Hz, under the following experimental conditions: 1) and 2) end-effector against a wall, with velocity reference amplitudes = 0.1 rad/s, and 0.2 rad/s, respectively; 3) end-effector holding a mass whose moment of inertia = 1.5 kg·m^2 around the rotational axis of the robot, with the mass attached to a wall with a spring whose spring constant = 3300 Nm/rad and whose damping is small and uncertain but estimated to be less than 10 Nm/(rad/s); 4), 5), and 6) end-effector attached to a mass whose moment of inertia = 2.4 kg·m^2, 4.6 kg·m^2, and 10.2 kg·m^2, respectively, and no spring attached. Case 1), $P_1(j\omega)$, was chosen as the nominal plant case. The transfer functions are displayed in Figure 3, and in Figure 4 as filled outlines of the value sets or templates $\{P_i(j\omega)\}$, i=1,…,6, for $\omega=2\cdot\pi\cdot$[1 2 5 8 10 15 20 22 24 33 40 46 50 55 63 70 80 99] rad/s. The sampling induced non-minimum phase characteristics of the plants can easily be discerned.

III. Robot Impedance Calculation

Here we wish to expound further on the method to calculate the robot impedance presented in [13]. Consider the robot part to the left of // in the block diagram in Figure 2, with G(s)=0. The robot may be seen as having two inputs, the motor velocity reference u [rad/s], and the end effector velocity v = dx_e/dt [rad/s] imposed by the environment, and

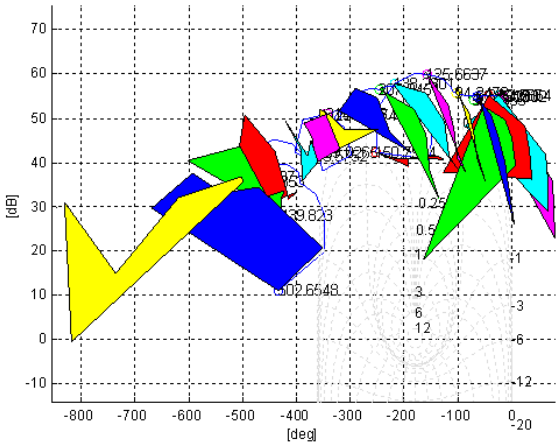

Fig. 4. The colored areas are outlines of the value sets or templates for the frequencies $2\cdot\pi\cdot$[1 2 5 8 10 15 20 22 24 33 40 46 50 55 63 70 80 99] rad/s in a Nichols diagram from the six experimentally measured frequency response functions, $P_i(j\omega)$, i=1,…,6 for the Stäubli RX90L robot attached to environments described in section V. The blue curve is $P_1(j\omega)$, chosen as the nominal, drawn for a dense set of frequencies.

one output, the end effector torque F_e [Nm]. The input-output relationship can be modeled linearly in the Laplace domain

$$F_e(s) = B(s)v(s) + A(s)u(s), \qquad (1)$$

where B(s) and A(s) are transfer functions. The robot impedance is defined as

$$Z(s) \stackrel{\text{def}}{=} - F_e(s)/v(s) \qquad (2)$$

and, clearly, with u=0 we get that the robot impedance with motor velocity control only is $Z_0(s)=-B(s)$. We now wish to show how B(s) and A(s) can be found from the performed frequency response experiments, and how the impedance, $Z_C(s)$ of the torque controlled robot (Figure 2) can be computed.

Letting v=0 by having the robot operate against a wall as in the frequency response experiments 1) and 2) above, yields A(s) in (1). In this paper we chose $P_1(s)=A(s)$.

It is well known that the environment admittance,

$$Y(s) \stackrel{\text{def}}{=} sx_h(s)/F_e(s), \qquad (3)$$

with $sx_h(s)=v(s)$ in the coupled system in Figure 2, of the spring-mass-(or moment of inertia)-damper environment to the right of // in Figure 2 is given by $Y(s)=s/(m_hs^2+b_hs+k_h)$. In e.g. experiment 3) above, an estimate of the environment admittance is $Y(s) = s/(1.5s^2+b_hs+3300)$, with $b_h<10$. With Y(s) and A(s) known, (1) and (3) yield $F_e(s) = B(s)Y(s)F_e(s) + A(s)u(s)$, or

$$F_e(s) = A(s)u(s)/(1- B(s)Y(s)) \stackrel{\text{def}}{=} H(s)u(s) \qquad (4)$$

Identifying the plant transfer function with u as input and F_e as output, when the robot acts against a known environment yields H(s). In this paper we chose the third experiment, i.e. $P_3(s)=H(s)$. From (4) one gets $B(s)=(H(s) – A(s))/(Y(s)H(s))$, and the robot impedance with motor velocity control only, $Z_0(s)=-B(s)$ is found.

With closed loop torque control, and $F_{eref}=0$, it holds that $u(s)=-G(s)F_e(s)$. Inserting the equation in (1) yields $F_e(s) = B(s)v(s)–A(s)G(s)F_e(s)$, or rearranged, $(1+A(s)G(s))F_e(s)= B(s)v(s)$ which together with (2) gives the impedance of the torque controlled robot with an inner motor velocity loop,

$$Z(s) = -B(s)/(1+A(s)G(s)) \qquad (5)$$

from which $Z_0(s)$ is also recovered by setting G(s)=0. Some examples of impedances computed this way are displayed below in Figure 6.

IV. Controller Design

In [13, fig. 4], a PI-controller is suggested for the torque feedback to motor velocity reference, $G_X(s) = k_P+k_I/s$ with $k_P=0.0005$, and $k_I= 0.07$, designed to sit on the passivity limit. In fact, passivity seems to be just slightly violated, see Figure 6 below.

Here we wish to compare with another controller, designed with Quantitative Feedback Theory (QFT) [15], [16]. Horowitz-Sidi bounds $B(j\omega)\in\mathbb{C}$ are computed from the closed loop sensitivity specification $|S(s)|\le 6$ dB, chosen in order to give satisfactory stability margins, and the plant templates (Figure 4), in such a way that if $L_{nom}(j\omega)= P_{nom}(j\omega)G(j\omega)$ satisfies $B(j\omega)$, then all closed loop cases satisfy the underlying sensitivity specification. Note that we did not postulate passivity as a design constraint. By manual loop shaping we found that the controller

$$G_P(s) = \frac{0.04\left(1+\frac{0.9s}{7}+\frac{s^2}{7^2}\right)\left(1+\frac{s}{33}\right)\left(1+\frac{s}{69}\right)\left(1+\frac{s}{500}\right)^2}{s\left(1+\frac{s}{7}\right)\left(1+\frac{s}{15}\right)\left(1+\frac{s}{18}\right)\left(1+\frac{s}{70}\right)\left(1+\frac{s}{258}\right)}$$

satisfy the Horowitz-Sidi bounds for a selected set of frequencies, and, more importantly, made the closed loop satisfy the sensitivity specification $|S(s)|\le 6$ dB for all six plant cases.

Figure 5 presents the two compensated nominal open loops $P_1(j\omega)G_X(j\omega)$ and $P_1(j\omega)G_P(j\omega)$ in a Nichols diagram, with the 6 dB sensitivity bounds for 3 and 18 Hz which

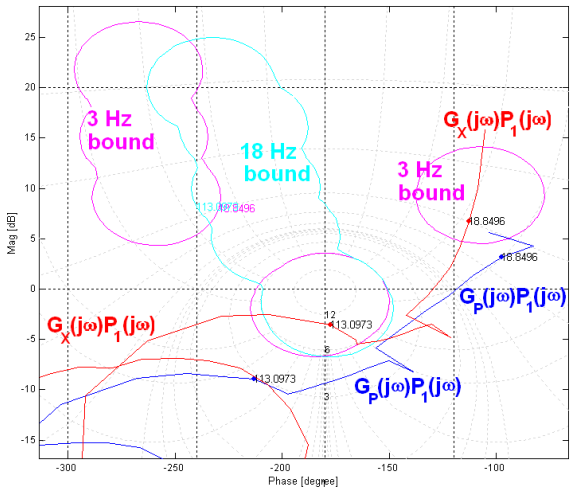

Fig. 5. Horowitz-Sidi bounds in a Nichols chart emanating from the sensitivity specification $|S(s)|\leq 6$ dB for [3, 18] Hz, together with the nominal compensated open loops $P_1(j\omega)G_P(j\omega)$ (blue), $P_1(j\omega)G_X(j\omega)$ (red), respectively, parameterized in rad/s.

$P_1(j\omega)G_X(j\omega)$ violate. Clearly the PI-design yields a gain margin of less than 3 dB, and it can be shown that its phase margin is about 10 deg, only – hence the closed loop is marginally stable. The high-order design $G_P(s)$ respects the 6 dB sensitivity specification for all plant cases and for all frequencies, and hence at least 6 dB gain margin and 30 deg phase margin is maintained.

The impedance of the robot with the closed motor velocity loop only, and the impedances of the robot with the velocity loop and the two torque control loops, respectively, are shown in Figure 6. It is seen that the impedance reduction from the velocity controlled robot is, for 1 Hz, 7 dB for the robot that is velocity controlled, and torque controlled with $G_P(s)$, and 16 dB for the robot that is velocity controlled, and torque controlled with $G_X(s)$. In that respect the PI-controller is superior. This will cause the apparent inertia of the PI-controlled robot to seem smallest for a human operator who is handling the robot, something that is demonstrated below.

However, while both the velocity controlled only robot, and the $G_P(s)$ controlled robot are clearly passive, the PI-controlled robot is marginally non-passive, as seen for

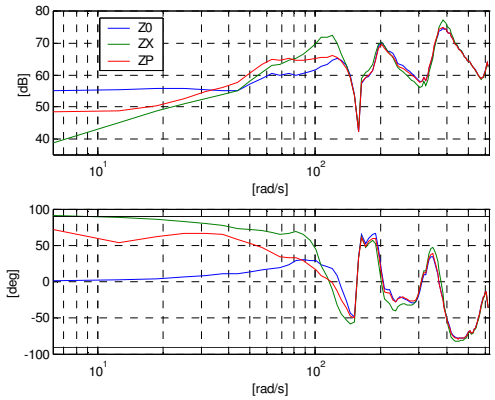

Fig. 6. The impedances for the robot controlled with the motor velocity loop only (Z0), with the velocity loop and the torque controller $G_X(s)$ (ZX), and with the velocity loop and the torque controller $G_P(s)$ (ZP).

frequencies lower than 3 Hz in the lower diagram in Figure 6 which depicts the phase.

The two torque controllers were implemented in digital form with the sampling frequency = 341.3 Hz, such that the digital frequency functions "overlapped" their respective analog transfer functions almost up to the Nyquist frequency, so called "matched" translation.

V. Evaluation Experiments

The first experiment to evaluate the performance of the two torque controllers was as follows. From a distance of about 5 cm, the robot arm was released and let free to coast towards a solid wall, corresponding to the identification cases 4, and 1 or 2, respectively. A small positive end-effector torque reference was given, F_{eref} = 4 Nm, see Figure 2, in order to make the robot arm stay in contact with the wall in steady state. Our study reveals the transient and steady state responses.

Figure 7 depicts the response when the PI-controller is active. The robot arm coasts to the wall for 0.6 seconds while the end effector torque is $F_e(t)=0$. Then the end effector hits the wall, F_e rises to 200 Nm, and the arm bounces, returns to wall at 1.2 seconds after the first bounce, and finally, after 6 bounces, comes to rest on the wall at time 4.4 seconds after the first bounce, and then $F_e = F_{eref}$ = 4 Nm.

In Figure 8 the time response is given when the high order controller $G_P(s)$ is used. The time axis is shifted relative to Figure 7 such that when the figures are put on top of each other, the first bounces occur simultaneously. The scales of all axes in Figure 8 are the same as in Figure 7. We note in Figure 8 that the robot arm coasts to the wall for 0.6 seconds, and after 2 minor bounces stays at the wall from 0.7 seconds after the first bounce. We get $F_e = F_{eref}$ = 4 Nm from 1.6 seconds after the first bounce. Clearly the $G_P(s)$-controlled robot is faster and more stable when in contact with a rigid environment.

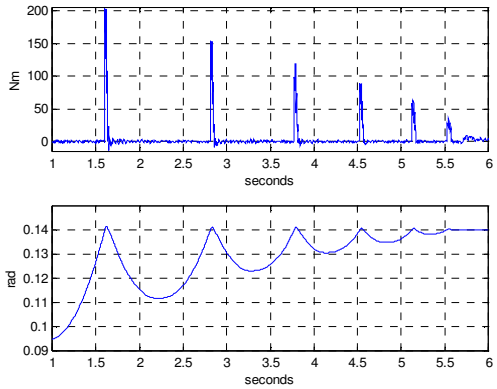

Fig. 7. The time response of the Stäubli RX90L robot with an inner motor velocity loop, and the end effector torque controlled by $G_X(s)$. The torque reference is F_{eref} = 4 Nm. The robot arm coasts towards a solid wall, and bounces 6 times before coming to rest. The upper graph shows the end effector torque $F_e(t)$ as a function of time, and the lower graph the motor encoder position reading as a function of time.

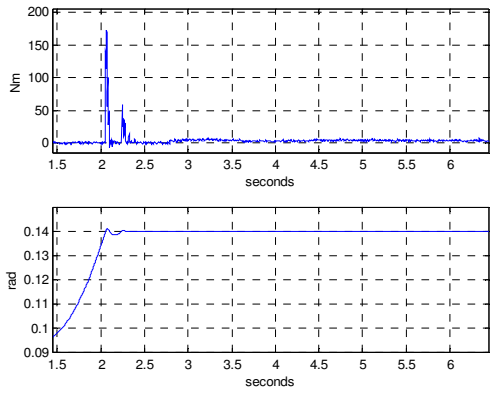

Fig. 8. The time response of the Stäubli RX90L robot with an inner motor velocity loop, and the end effector torque controlled by $G_P(s)$. The torque reference is F_{eref} = 4 Nm. The robot arm coasts towards a solid wall, and bounces twice before coming to rest. The upper graph shows the end effector torque $F_e(t)$ as a function of time, and the lower graph the motor encoder position reading as a function of time.

The second experiment was to attach the torque controlled robot end effector to a spring-mass-damper whose other end was attached to a wall. The spring constant was 3670 Nm/rad, and the moment-of-inertia and damper were unknown but similar to those of identification experiment 3). F_{eref} was set to zero. Before the experiment the closed loop system was in equilibrium. The end effector was slightly moved, and the transient response to the thus created non-equilibrium initial condition was recorded, in Figure 9 when $G_X(s)$ was in control, and in Figure 10 with $G_P(s)$ in charge. Clearly $G_X(s)$ does not stabilize this closed loop system, and is thus not robust to the design environments. It should be pointed out, however, that by slightly lowering the integral gain k_I, it was possible to achieve stability while the controlled robot was still marginally non-passive, but with an unsatisfactorily slow convergence to equilibrium.

The last experiment was as follows. F_{eref} was set to zero, and a human operator moved the robot end-effector rhythmically in a sinus-like fashion with a peak-peak amplitude of about 0.5 rad. The controller was changed suddenly from $G_X(s)$ to $G_P(s)$ and vice versa a number of times. The effort the human operator exerts is an increasing function of $F_e(t)$. $F_e(t)$ is displayed in Figure 11. Clearly, the effort, or "apparent inertia" during the periods when $G_P(s)$ was used was more than double the effort when $G_X(s)$ was used.

VI. Discussion and Conclusions

Standard robust control engineering practice demands that a closed loop system be designed such that reasonable stability margins are maintained for all plant cases, normally at least 6 dB gain margin and 30 deg phase margin, or $|S(s)| \leq 6$ dB, even when all known or assumed plant uncertainty, including environment uncertainty, is taken into account in the design process. On the other hand, some robot control designers seem to reason that if the controlled robot is made passive, then coupled stability is ensured with all passive environments also without stability margins, and that this "insight" can be transferred to the case when passivity is abandoned in view of bounded environment uncertainty and more exacting performance specifications.

Our examples demonstrate that controlled robot passivity "happens" by itself if the environment uncertainty includes a set of cases that require passivity, and that stability margins are necessary for good performance even when the controlled robot is passive. Clearly, controlled robot passivity need not necessarily be a design constraint, but stability margins are mandatory.

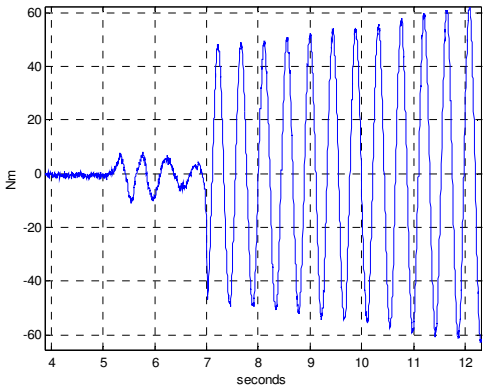

Fig. 9. The torque response $F_e(t)$ as a function of time of the Stäubli RX90L robot with an inner motor velocity loop, and the end effector torque controlled by $G_X(s)$. The torque reference is F_{eref} = 0 Nm. The robot arm is attached to a spring with a small mass and small damping, and the other end of the spring is attached to a wall. The end effector was moved out of equilibrium, and the transient torque response was unstable.

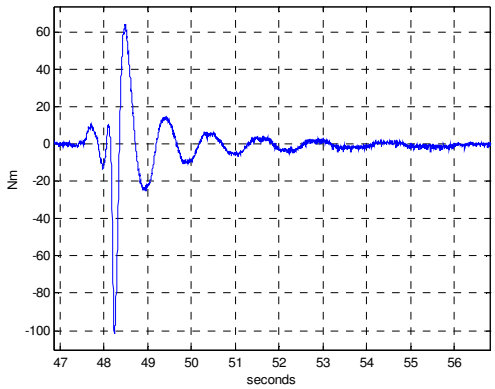

Fig. 10. The torque response $F_e(t)$ as a function of time of the Stäubli RX90L robot with an inner motor velocity loop, and the end effector torque controlled by $G_P(s)$. The torque reference is F_{eref} = 0 Nm. The robot arm is attached to a spring with a small mass and small damping, and the other end of the spring is attached to a wall. The end effector was moved out of equilibrium, and the exponentially stable transient torque response is displayed.

The drawback of the robust controller is that demands a substantially higher effort by an operator handling the robot than the marginally non-stabilizing controller. From a control theoretic point of view, this is not surprising: it is well known that unstable systems are more agile than stable ones, e.g. modern fighter airplanes are designed to be inherently unstable.

While this paper does not advocate any specific method of design, and contains mainly more details and experiments beyond those reported in [2] and [13], it contributes to point out the importance of analyzing and reporting stability margins which is often not done in the robotics literature when e.g. Lyapunov function type stability arguments are used.

It seems reasonable to argue that the conflict between robustness and low impedance gain for easy robot handling in cobotics cannot be resolved by including the human arm in the set of passive environments for which the robust design is made. One interesting and potentially useful approach is suggested in [17] where a non-linear sliding mode controller is developed. Another solution might be a kind of "gain scheduling", i.e. to have a sensor indicating the presence of a human handler, and design a controller suited for that situation, while the robust controller is active when the environment is non-human, with a "bumpless" transfer between the two controllers. Research along these lines is in progress.

ACKNOWLEDGMENT

The support of CEA is gratefully acknowledged by the first and last authors who hold guest positions at CEA.

REFERENCES

[1] S. Buerger and N. Hogan, "Complementary Stability and Loop Shaping for Improved Human–Robot Interaction," *IEEE Transactions on Robotics,* vol. 23, April 2007, pp. 232-244.

[2] X. Lamy, F. Colledani, and P.-O. Gutman, "Stability margins and passivity for the control of robots operating in varying-impedance environments," Proceedings *18th Mediterranean Conference on Control and Automation*, June 23-25, 2010, Marrakech, Morocco.

[3] D. Surdilovic, "Robust control design of impedance control for industrial robots," *IEEE/RSJ International Conference on*, *Intelligent Robots and Systems, 2007. IROS 2007.* 2007, pp. 3572-3579.

[4] Maolin Jin, Sang Hoon Kang, and Pyung Hun Chang, "Robust Compliant Motion Control of Robot With Nonlinear Friction Using Time-Delay Estimation," *IEEE Transactions on Industrial Electronics,* vol. 55, 2008, pp. 258-269.

[5] J. Hart and G. Niemeyer, "Model-reference based wave-variable force control," *IEEE International Conference on Robotics and Automation, 2009. ICRA '09.* 2009, pp. 4074-4079.

[6] K. Kosuge, Y. Fujisawa, and T. Fukuda, "Interface Design for Man-Machine Mechanical Interactions," *Proceedings IEEE International Workshop on.Robot and Human Communication,* 1992.

[7] J. Colgate, M. Peshkin, and S. Klostermeyer, "Intelligent assist devices in industrial applications: a review," *Proceedings 2003 IEEE/RSJ International Conference on Intelligent Robots and Systems, 2003* (*IROS 2003*), vol.3, 2003, pp. 2516-2521.

[8] J. Krüger and D. Surdilovic, "Robust control of force-coupled human-robot-interaction in assembly processes," *CIRP Annals - Manufacturing Technology*, vol. 57, 2008, pp. 41-44.

[9] N. Hogan, "Impedance Control:An Approach to Manipulation, Parts I,II,III ," *ASME Journal of Dynamic Systems, Measurement and Control*, vol. 107, 1985, pp. 1-24.

[10] N. Hogan, "Controlling impedance at the man/machine interface," *Proceedings 1989 IEEE International Conference on on Robotics and Automation*, Scottsdale, AZ, 1989, pp. 1626 - 1631.

[11] J.E. Colgate and N. Hogan, "Robust control of dynamically interacting systems," *International Journal of Control*, vol. 48, July 1988, pp. 65 - 88.

[12] W.S. Newman, "Stability and Performance Limits of Interaction Controllers," *Journal of Dynamic Systems, Measurement, and Control*, vol. 114, Dec.1992, pp. 563-570.

[13] X. Lamy, F. Colledani, F. Geffard, Y. Measson, and G. Morel, "Achieving efficient and stable comanipulation through adaptation to changes in human arm impedance," *IEEE International Conference on Robotics and Automation, 2009. ICRA '09*, 2009, pp. 265-271.

[14] L. Ljung (1987), *System Identification – Theory for the User*, Englewood Cliffs, New Jersey: Prentice-Hall.

[15] Horowitz I. (1992), *Quantitative Feedback Design Theory (QFT)* , vol 1, Boulder, Colorado: QFT Publications, 1992.

[16] P-O. Gutman, *Qsyn* - the *Toolbox for Robust Control Systems Design for use with Matlab, User's Guide*. Rehovot, Israel El-Op Electro-Optics Industries Ltd,1996. Also available at http://www.math.kth.se/optsyst/research/5B5782/index.html

[17] R. Kikuuwe, H. Fujimoto, "Proxy-based sliding mode control for accurate and safe position control ," *Proceedings 2006 IEEE International Conference on Robotics and Automation (ICRA 2006)*, 2006, pp. 25-30.

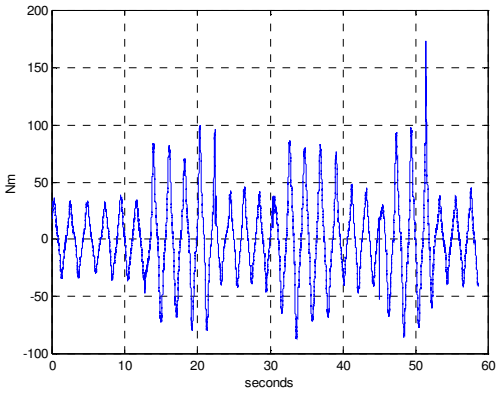

Fig. 11. The torque response $F_e(t)$ as a function of time of the Stäubli RX90L robot with an inner motor velocity loop, and the end effector torque controlled by intermittently $G_P(s)$ and $G_X(s)$, when the robot end-effector is moved by a human operator in a sinus-like fashion with peak-peak amplitude ≈ 0.5 rad, while the torque reference is F_{eref} = 0 Nm. The time intervals when the peak torque is low corresponds to the periods when $G_X(s)$ was used.